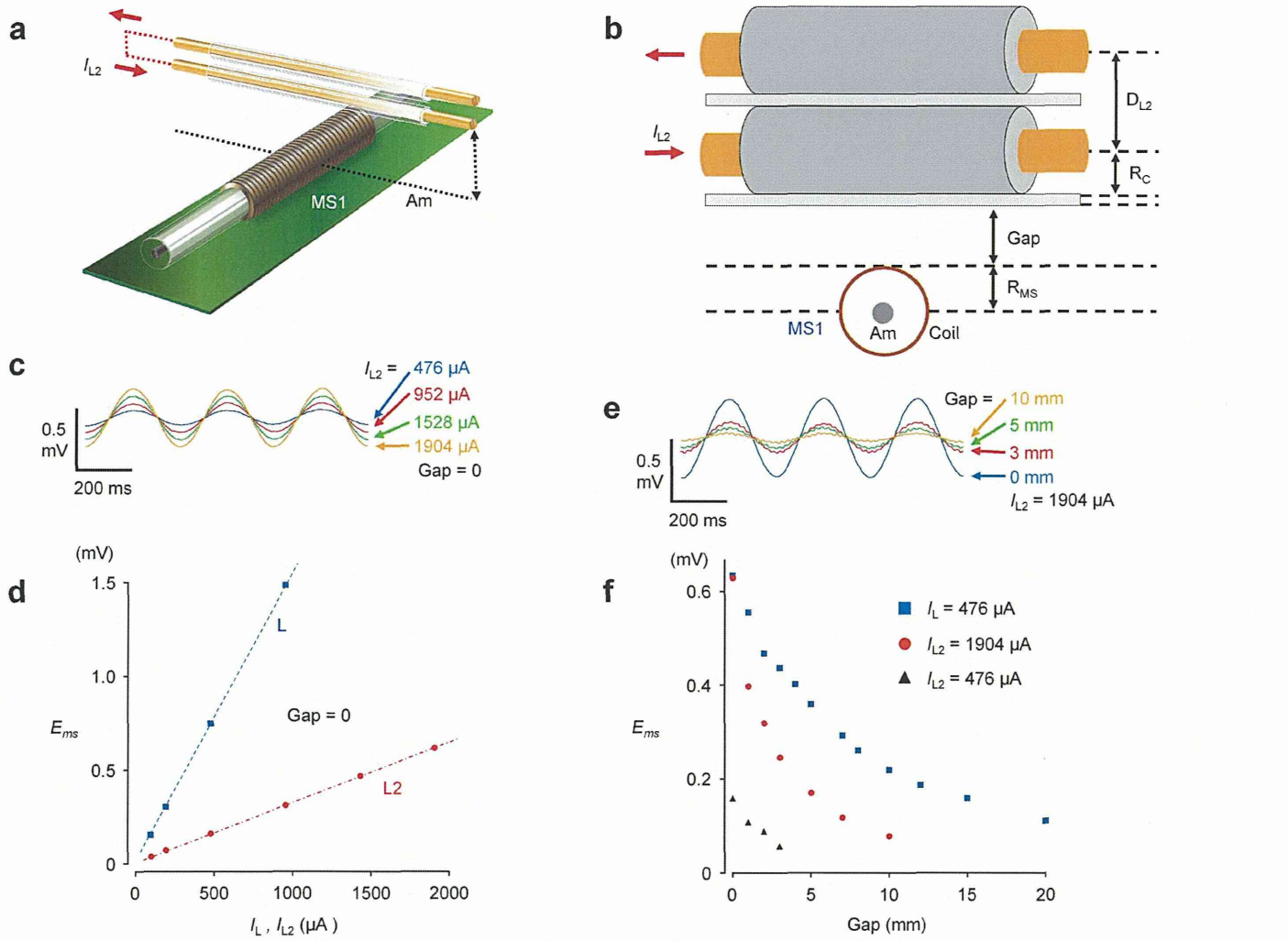

Figure 5 | Practical model of a biomagnetic field. (a,b) A pair of linear insulated electric cables (30 cm in length, 0.5 mm in radius: R_c) are piled on top of an MS1 magneto sensor and separated by a cover glass plate (100 μm thick). The distance between the two cables (D_{L2}) is ~1.1 mm. Various amplitudes of current (I_{L2}) were applied to the paired cables, which were raised with various gaps. (c,d) Changes in the output voltage of the magneto sensor amplifier (E_{ms}) by applying various I_{L2} with no gaps. (e,f) Changes in E_{ms} by shifting the I_{L2} gap distance by 1904 μA. The results of single cable (Fig. 2 d and f: I_L = 476 μA) are reproduced to show the difference. Also, in (f), changes in E_{ms} with an I_{L2} of 476 μA are shown.

sensor with a higher spatial resolution, such as a multi-channel amorphous metal-based magneto sensor, and by using more accurate models of an effective circuit (Fig. S7).

Special pacemaker cells are known to exist in the ileum, and play an essential role in generating spontaneous electric activity. From histological features, the pacemaker cells are referred to as interstitial cells of Cajal (ICC)[15,16]. However, in light of the distinct expression of ion channels, the TEA facilitation of biomagnetic waves is ascribed to an electric current in the smooth muscle. 1) In smooth muscle cells, TEA blocks a major K^+ current, and also amplifies intracellular Ca^{2+} transients, both being known to enhance excitability[17–19]. On the other hand, a TEA-insensitive K^+ current plays a major role in regulating pacemaker activity in ICC[20]. 2) Upon depolarization, L-type Ca^{2+} channels ($Ca_v1.2$) are responsible for a voltage-gated inward current in smooth muscle[21,22], while T-type Ca^{2+} channels ($Ca_v3.2$) as well as TTX-insensitive voltage-gated Na^+ channels are suggested to play a major role in ICC pacemaking[23,24]. The fact that application of nifedipine, an L-type Ca^{2+} channel-specific blocker, abolishes biomagnetic waves in the presence of TEA (Fig S3), reinforces a predominant contribution of smooth muscle electric current to intercellular electric current under normal conditions. It is considered that although ICC pacemaker current underlies smooth muscle spontaneous activity[25,26], a major component of electric current propagating through the muscle layer is regenerated in smooth muscle cells.

To date, SQUID has been employed as a major tool to measure biomagnetic fields, such as magnetoencephalography and magnetocardiography[4,27–29]. Recently, atomic magnetometers utilizing vapors of polarized alkaline metals (Rb, Cs and K) have become popular as an alternative tool[5,30,31]. These two magnetometers are currently available for biomagnetic field measurements. The former is a vector magnetometer, while the latter is a scalar magnetometer. Therefore, only the former SQUID magnetometer is available for measuring biomagnetic vector fields, similar to the present measurements. Since the former and latter are normally operated at extremely low and high temperatures, respectively, compared to body temperature, sensor devices are mounted in containers separated from biological systems. SQUID microscopy with small pickup coils (500 μm in diameter) has been applied to an isolated whole heart to measure electric stimulation-evoked magnetic fields with a sub-pT range

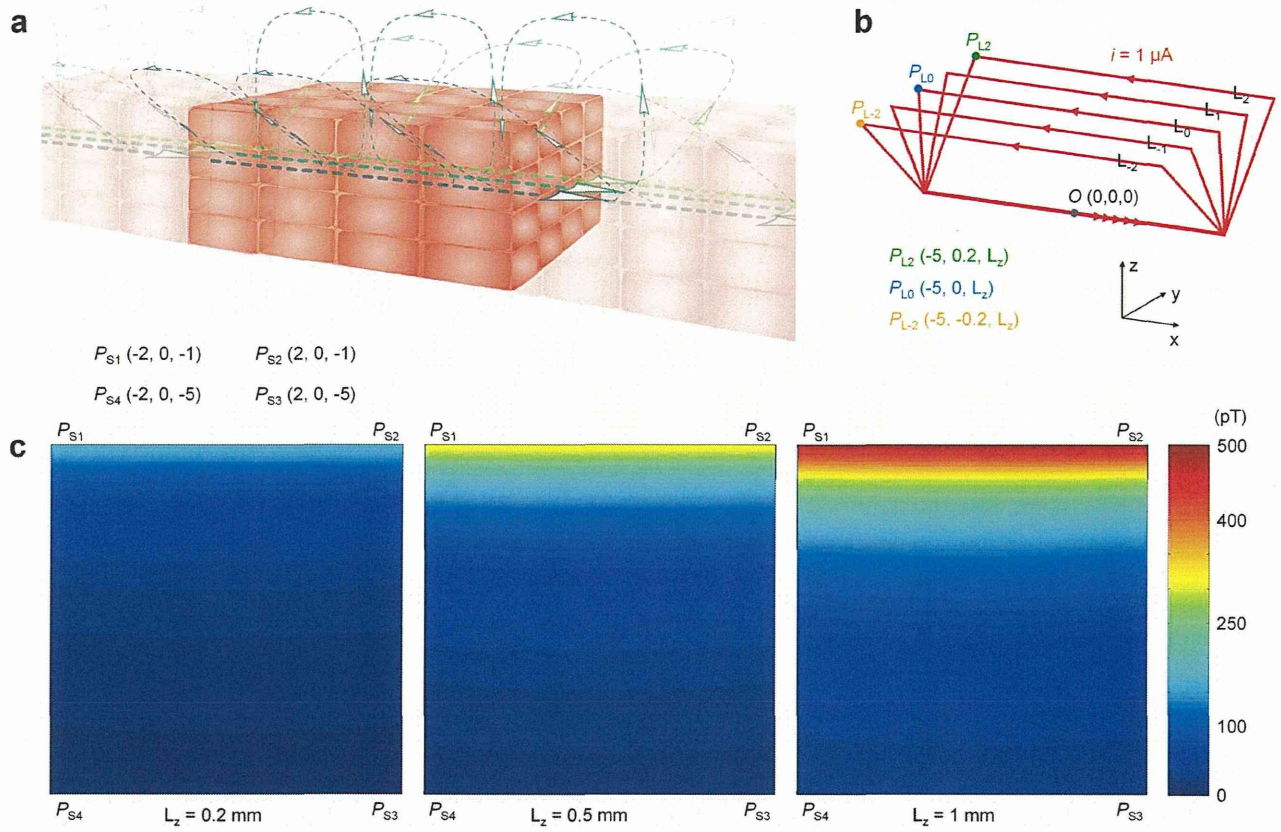

Figure 6 | Computer simulation of a biomagnetic field. (a) An illustration of cellular organizations with intercellular propagating current and extracellular return current. The return current may consist of intercellular currents towards surface cells as well as extracellular surface currents. (b) Simplified circuits for simulation of a biomagnetic field. Five electric circuits (L_{-2} to L_2) are combined and a 1 μA current is conducted in each circuit. In brackets, x, y and z coordinates of points in the circuit are indicated in mm. The distance of current propagation corresponds to ~60 cells in a longitudinal direction, assuming a cell length of 150 μm. (c) Biomagnetic field maps of L_z = 0.2, 0.5 and 1 mm. P_{S1} – P_{S4} are the four corners of the map. Note the amplification of the magnetic field by increasing the L_z distance of the circuit.

sensitivity[32,33]. More recently, atomic magnetometers operated at a room temperature have been reported, but sensitivity is similarly reduced[34]. Also, both magnetometers require a magnetic shield to reduce the environmental magnetic field within a maximal detection limit. Therefore, the total system becomes large in these magnetometers.

In the light of the present experiments, we propose a new option to measure biomagnetic fields, depending on the aim and objective of study. The gradiomagneto sensor device used herein is made of an amorphous metal wire and ordinary electro-magnetic materials, and is operated at ambient temperature. Thus, our sensor can be placed very close to the sample, and can also detect the magnetic fields of a limited region that corresponds to the volume of the amorphous metal wire. On the other hand, magnetometers with very high sensitivity, such as SQUID and atomic magnetometers, have the same average volume of detector coils and vapor containers, respectively. Also, amorphous metal-based sensors do not require any magnetic shield against geomagnetic fields, because voltage conversion of the magnetic field is linear over a range of ±50 μT[9]. For these reasons, our magneto sensor is applied to measure small biological samples, and can be compacted for portable use.

Details of single cell and single ionic channel properties are now being elucidated due to the development of micromanipulation and fine voltage-clamp technologies[35]. In contrast, electric properties of cellular organizations remain unknown. Since innumerous electric syncytia of excitable cells with intercellular electric coupling, exist over the entire human body, such information enables the evaluation of integrated functions of biological systems. The magneto sensor used in this study could be a good tool for such a purpose. Also, in regenerative medicine, magneto sensors with high sensitivity may be useful for aseptic and non-invasive evaluations of spatial activity in cellular tissue samples derived from stem cells[36,37]. Especially, for small samples of biological systems, magneto sensors that can closely approach the sample are advantageous to detect magnetic fields, because biomagnetic fields induced in small circuits rapidly decline even over a small distance (Fig. 6c).

The sensitivity and stability of amorphous material-based magnetic sensors are expected to improve further with additional development[38]. The intrinsic noise of the sensor is estimated to be less than 10 fT/$\sqrt{}$ (Hz) in the same sized wire used in this study, assuming the electron spin density of a typical Co-rich amorphous metal without a significant magnetic domain movement[39–41]. Therefore, in order to improve this magneto sensor, it is crucial to use uniformly manufactured paired transducer coils designed for amorphous metal materials, and to find good amorphous metal materials and electric devices that more efficiently convert excitation-pulse-induced induction potentials into the signal output of a magnetic field[42]. Also, amorphous metal-based magneto sensors could be developed as micro-electro mechanical system (MEMS)-like integrated circuits, thus allowing the total apparatus to be compacted for use in small labs, hospitals and even for home use, without using any magnetic shield. In initial studies of biological electric activity, such as electrocardiograms, measurements were carried out using a galvanometer, which converts changes in a magnetic field

to induction potentials, a remind that measurements of biological magnetic and electric fields are closely related. Unfortunately, at present, biomagnetic field measurements are performed at only a few sites, while portable bioelectric detectors are available in electrocardiography and electroencephalography. We anticipate that amorphous metal-based magneto sensor technology would make biomagentic fields a more realistic aspect in our lives, and that this technology could be employed to make new detectors for biological and medical samples, depending on the aim and objective of the study.

Methods

Magneto sensor. The set of panels in Fig. 1 shows the amorphous metal-based gradio-magneto sensor system used in the present study. To improve the gradio-sensing of a magnetic field, a pair of transducer solenoid coils (0.5 mm in radius; 10 mm in length; 300 turns) was mounted at both ends of a single amorphous (Am) wire (30 μm in diameter, ~50 mm in length) of no magnetostriction. The composition of the wire used was (in atomic percentages): Co-F alloy (94 *vs* 6) 72.5; Si 12.5; B 15. Presumably, due to the symmetrical magnetic fields distributed along the amorphous wire, the induction potentials in the paired transducer coils were much more identical in terms of the amplitude and decay time course, compared with those induced in a pair of separated magneto-impedance (MI) elements previously used[6,7].

The driving and detecting devices were as follows: A clock CMOS IC triggers a pulse gate (PG) CMOS IC that supplies electric excitation pulses (P_e) of 5 V (100 ns) to the magnetic amorphous wire at 2 μsec intervals. The intermediate portion of the wire was electrically shunted with an electric cable in order to reduce the resistance of the excitation circuit to ~50 Ω. The same clock IC simultaneously triggers a pair of sample-and-hold circuits (SH1, SH2) to detect the induction potential of the coils in MS1 and MS2 magneto detectors. The detection devices for the paired coils were essentially similar to those used previously[6,7] (See Fig S1 for magneto detection mechanisms).

High-speed operation amplifiers with a frequency range of several MHz were used to follow and differentiate the SH1 and SH2 voltages (subtracting the induction potential of SH2 from that of SH1) to cancel environmental magnetic noise. Also, the differentiated signal was amplified ~1000 times. After the operation amplifiers, high and low cut electric filters (H/L filter: 20 and 0.3 Hz, respectively) were applied, and the resulting voltage output was sampled to computer memory through a data logger with a frequency of 1 kHz. Positive (upward) signals in figures represent the direction of the magnetic field from MS2 to MS1.

Specifications of the gradio-type magneto sensor were assessed using a model system. A linear electric cable 1 mm in diameter and 30 cm in length was crossed on MS1 at the center, and oscillating electric currents (sine waves) were applied at 3 Hz (Fig. 2). The magnetic field (output voltage) detected progressively decreased as the distance between the electric cable and MS1 increased. The conversion efficacy of magnetic field into output voltage was estimated to be ~25 μV/nT (~0.031 V/A/m, i.e. $B = \mu_0 H$, and $\mu_0 = 1.256 \times 10^{-6}$ T/A/m). The noise level was ~30 pT/Hz$^{1/2}$. Also, the performance of the subtraction (gradio-sensing) between MS1 and MS2 was assessed by changing the amplitude and frequency of the external magnetic field, when the whole sensor system was placed in a Helmholz coil of 30 cm diameter. The output potentials of SH1 and SH2 differ at most by ~3% at 1–20 Hz.

Animals and preparations. Animals were treated ethically, in accordance with the guidelines for proper conduct of animal experiments by the Science Council of Japan. All procedures were approved by the Animal Care and Use Committee of Nagoya University Graduate School of Medicine (Permission #23357). Guinea pigs of ~3 weeks after birth were killed by cervical dislocation and exsanguination after deeply anaesthetising with diethyl ether. Smooth muscle tissues were isolated with a pair of fine scissors. For magnetic measurements connective tissue and the mucous membrane were carefully removed using forceps and fine scissors under a binocular microscope (SZ61, Olympus, Tokyo, Japan).

Measurements of biological magnetic field. Musculatures isolated from the ileum (~5 mm wide × 25–35 mm long × 0.5–1 mm thick) were mounted in a recording chamber with the bottom of a cover glass of 100 μm thick, using a tissue anchor rig made by thin strings (SDH series, Harvard Apparatus Japan, Tokyo, Japan). The chamber contained a 'normal' extracellular solution kept at 34–36°C using a plastic panel heater in which warm water was sufficiently circulated before measurements (Fig. 3a).

Changes in magnetic fields were measured along the amorphous wire by discriminating the direction. One of the paired magneto detectors (MS1 in Fig. 1 a) was placed below the recording chamber, while the other (MS2) magneto detector at the other end of the amorphous wire was used to sense the environmental magnetic field. The differentiated potential of MS2 from MS1 after the sample-and-hold circuits was recorded as biomagnetic fields arising from ileal musculature samples.

In some experiments, pharmacological interventions were carried out in order to enhance or suppress biological magnetic (and electric) activity (Figs. 3 and 4; Fig. S3).

Solutions and drugs. The composition of the 'normal' extracellular solution (modified Krebs solution) used, was (in mM): NaCl 125; KCl 5.9; $MgCl_2$ 1.2; $CaCl_2$ 2.4; glucose 11; Tris-HEPES 11.8 (pH 7.4). TEA was purchased from Sigma-Aldrich (St Louis, MO, USA).

Simulation. A practical model of a biological magnetic field was made with a pair of electric cables (1 mm in diameter; 30 cm in length) with a center distance of ~1100 μm (Fig. 5). Magnetic fields were measured using the gradio-magneto sensor by changing the amplitude of the oscillating electric current and the distance between the cable and MS1.

In computer simulation, the magnetic field in a certain point was estimated using the 'P and Qm' software package, by integrating a current-element-induced magnetic field along the electric circuit according to Biot-Savart law (Shift Lock Corp., Kishiwada, Japan). Pseudo-color magnetic field maps were drawn using MATLAB software (MathWorks, Arkansas Garden City, USA).

Data analysis. Digital band-pass filter, and linear spectrum analysis were performed using commercial add-in software (Kyowa Electronic Instruments, Tokyo, Japan). In histogram analysis, recording data of magnetic fields thinned out by 1/10, and 5000 data points (corresponding to 50 sec) were used. Histograms were constructed with a bin width of 5 pT, and plotted with cumulative curves (Fig. S2).

Numerical data are expressed as means ± S.D. Significant differences were evaluated by paired *t*-tests ($P < 0.05$).

1. Szurszewski, J. H. Electrical basis for gastrointestinal motility in *Physiology of Gastrointestinal Tract 2nd edn* (ed. Johnson, L. R.) 383–422 (Raven, 1987).
2. Tomita, T. Electrical activity (spikes and slow waves) in gastrointestinal smooth muscle in *Smooth Muscle: An Assessment of Current Knowledge* (eds. Bülbring, E., Brading, A. F., Jones, A. W. & Tomita, T.) 127–156 (Edward Arnold, 1981).
3. Wikswo, J. P. & Freeman, J. A. Magnetic field of a nerve impulse: First measurements. *Science* **208**, 53–55 (1980).
4. Williamson, S. J., Lü, Z. L., Karron, D. & Kaufman, L. Advantages and limitations of magnetic source imaging. *Brain Topogr.* **4**, 169–180 (1991).
5. Budker, D. & Romalis, M. Optical magnetometery. *Nat. Phys.* **3**, 227–234 (2007).
6. Nakayama, S., Atsuta, S., Shinmi, T. & Uchiyama, T. Pulse-driven magnetoimpedance sensor detection of biomagnetic fields in musculatures with spontaneous electric activity. *Biosens. Bioelectron.* **27**, 34–39 (2011).
7. Uchiyama, T., Mohri, K. & Nakayama, S. Measurement of spontaneous oscillatory magnetic field of guinea-pig stomach muscle preparation using pico-Tesla resolution amorphous wire magneto-impedance sensor. *IEEE Trans. Magn.* **47**, 3070–3073 (2011).
8. Nakayama, S. *et al.* Pacemaker phase shift in the absence of neural activity in guinea-pig stomach: a microelectrode array study. *J. Physiol.* **576**, 727–738 (2006).
9. Mohri, K. *et al.* Amorphous wire and CMOS-based sensitive micromagnetic sensors utilizing magneto-impedance (MI) and stress-impedance (SI) effects. *IEEE Trans. Magn.* **38**, 3063–3068 (2002).
10. Abe, Y. & Tomita, T. Cable properties of smooth muscle. *J. Physiol.* **196**, 87–100 (1968).
11. Tanaka, S. *et al.* Measurement of the signal from a cultured cell using a high-Tc SQUID. *Supercond. Sci. Technol.* **16**, 1536–1539 (2003).
12. Murdick, R. A. & Roth, B. J. A comparative model of two mechanisms from which a magnetic field arises in the heart. *J. Appl. Phys.* **95**, 5116–5122 (2004).
13. Bolton, T. B. Effects of stimulating the acetylcholine receptor on the current-voltage relationships of the smooth muscle membrane studied by voltage clamp of potential recorded by micro-electrode. *J. Physiol.* **250**, 175–202 (1975).
14. Tomita, T. Membrane capacity and resistance of mammalian smooth muscle. *J. Theoret. Biol.* **12**, 216–227 (1966).
15. Sanders, K. M. *et al.* Development and plasticity of interstitial cells of Cajal. *Neurogastroenterol. Motil.* **11**, 311–338 (1999).
16. Furness, J. in *The enteric nervous system 1st edn.* 1–288 (Wiley-Blackwell, 2006).
17. Muraki, K. *et al.* Effects of tetraethylammonium and 4-aminopyridine on outward currents and excitability in canine tracheal smooth muscle cells. *Br. J. Pharmacol.* **100**, 507–515 (1990).
18. Farrugia, G., Rae, J. L. & Szurszewski, J. H. Characterization of an outward potassium current in canine jejunal circular smooth muscle and its activation by fenamates. *J. Physiol.* **468**, 297–310 (1993).
19. Borisova, L., Shmygol, A., Wray, S. & Burdyga, T. Evidence that a Ca^{2+} sparks/STOCs coupling mechanism is responsible for the inhibitory effect of caffeine on electro-mechanical coupling in guinea pig ureteric smooth muscle. *Cell Calcium* **42**, 303–311 (2007).
20. Zhu, Y. *et al.* ERG K^+ currents regulate pacemaker activity in ICC. *Am. J. Physiol. Gastrointest. Liver Physiol.* **285**, G1249–1258 (2003).
21. Nakayama, S. *et al.* Tyrosine kinase inhibitors and ATP modulate the conversion of smooth muscle L-type Ca^{2+} channels toward a second open state. *FASEB J.* **20**, 1492–1494 (2006).
22. Akbarali, H. I., Hawkins, E. G., Ross, G. R. & Kang, M. Ion channel remodeling in gastrointestinal inflammation. *Neurogastroenterol. Motil.* **22**, 1045–1055 (2010).
23. Strege, P. R. *et al.* Effect of mibefradil on sodium and calcium currents. *Am. J. Physiol. Gastrointest. Liver Physiol.* **289**, G249–253 (2005).
24. Gibbons, S. J. *et al.* The alpha1H Ca^{2+} channel subunit is expressed in mouse jejunal interstitial cells of Cajal and myocytes. *J. Cell. Mol. Med.* **13**, 4422–4431 (2009).

25. van Helden, D. F. & Imtiaz, M. S. Ca^{2+} phase waves: a basis for cellular pacemaking and long-range synchronicity in the guinea-pig gastric pylorus. *J. Physiol.* **548**, 271–296 (2003).
26. Sperelakis, N. & Daniel, E. E. Activation of intestinal smooth muscle cells by interstitial cells of Cajal in simulation studies. *Am. J. Physiol. Gastrointest. Liver Physiol.* **286**, G234–243 (2004).
27. Cohen, D., Norman, J. C., Molokhia, F. & Hood, Jr. W. Magnetocardiography of direct currents: S-T segment and baseline shifts during experimental myocardial infarction. *Science* **172**, 1329–1333 (1971).
28. Koch, H. Recent advances in magnetocardiography. *J. Electrocardiol.* **37** Suppl, 117–122 (2004).
29. Soekadar, S. R. *et al.* In vivo assessment of human brain oscillations during application of transcranial electric currents. *Nat. Commun.* **4**, 2032; DOI:10.1038/ncomms3032 (2013).
30. Kamada, K., Ito, Y. & Kobayashi, T. Human MCG measurements with a high-sensitivity potassium atomic magnetometer. *Physiol. Meas.* **33**, 1063–1071 (2012).
31. Johnson, C. N., Schwindt, P. D. & Weisend, M. Multi-sensor magnetoencephalography with atomic magnetometers. *Phys. Med. Biol.* **58**, 6065–6077 (2013).
32. Baudenbacher, F., Peters, N. T., Baudenbacher, P. & Wikswo, Jr. J. P. High resolution imaging of biomagnetic fields generated by action currents in cardiac tissue using a LTS-SQUID microscope. *Physica C* **368**, 24–31 (2002).
33. Baudenbacher, F., Peters, N. T. & Wikswo, Jr. J. P. High resolution low-temperature superconductivity superconducting quantum interference device microscope for imaging magnetic fields of samples at room temperatures. *Rev. Sci. Instrum.* **72**, 1247–1254 (2002).
34. Sander, T. H. *et al.* Magnetoencephalography with a chip-scale atomic magnetometer. *Biomed. Opt. Express* **3**, 981–990 (2012).
35. Hamill, O. P. *et al.* Improved patch-clamp techniques for high-resolution current recording from cells and cell-free membrane patches. *Pflügers Arch.* **391**, 85–100 (1981).
36. Nelson, T. J., Martinez-Fernandez, A. & Terzic, A. Induced pluripotent stem cells: developmental biology to regenerative medicine. *Nat. Rev. Cardiol.* **7**, 700–710 (2010).
37. Itzhaki, I. *et al.* Modelling the long QT syndrome with induced pluripotent stem cells. *Nature* **471**, 225–229 (2011).
38. Vazquez, M. *et al.* On the state-of-the-art in magnetic microwires and expected trends for scientific and technological studies. *Phys. Status Solidi A* **208**, 493–501 (2011).
39. Melo, L. G. C. *et al.* Optimization of the magnetic noise and sensitivity of giant magnetoimpedance sensors. *J. Appl. Phys.* **103**, 033903; DOI:10.1063/1.2837106 (2008).
40. Ding, L. *et al.* Equivalent magnetic noise limit of low-cost GMI magnetometer. *IEEE Sensors J.* **9**, 159–168 (2009).
41. Gudoshnikov, S. *et al.* Highly sensitive magnetometer based on the off-diagonal GMI effect in Co-rich glass-coated microwire. *Phys. Status Solidi A* **211**, 980–985 (2014).
42. Uchiyama, T. & Nakayama, S. Magnetic sensors using amorphous metal materials: Detection of premature ventricular magnetic waves. *Physiol. Rep.* **1**, e00030; DOI:10.1002/phy2.30 (2013).

Acknowledgments

The authors are grateful to Ms Naoko Iwata and Megumi Tsutsui (Nagoya University) for processing data and drawing simulations, and to Mr Hideki Miyazaki, Yoshitaka Taguchi, Satoshi Atsuta, Shinsuke Kato and Yasutaka Shimizu (Fujidenolo Corp) for illustrations, and to Professors Joseph F. Clark (Cincinnati University) and Susan Wray (University of Liverpool) for proofreading and valuable discussion. This work was partly supported by research grants from the Japan Society for the Promotion Science (JSPS), and the New Energy and Industrial Technology Development Organization (NEDO).

Author contributions

S.N. designed this study, performed experiments, and wrote the manuscript. T.U. produced magneto sensors.

Additional information

Supplementary information accompanies this paper at http://www.nature.com/scientificreports

Competing financial interests: The authors declare no competing financial interests.

How to cite this article: Nakayama, S. & Uchiyama, T. Real-time Measurement of Biomagnetic Vector Fields in Functional Syncytium Using Amorphous Metal. *Sci. Rep.* 5, 8837; DOI:10.1038/srep08837 (2015).

MADE IN JAPAN